# Hydrogen production by methanol steam reforming on NiSn/MgO–Al2O3 catalysts: The role of MgO addition

A. Penkova (a), L. Bobadilla (a), S. Ivanova (a), M.I. Domínguez (a), F. Romero-Sarria (a), A.C. Roger (b), M.A. Centeno (a), J.A. Odriozola (a)

(a) Departamento de Química Inorgánica e Instituto de Ciencia de Materiales de Sevilla, Centro Mixto Universidad de Sevilla, CSIC, Avda Americo Vespucio 49, 41092 Seville, Spain

(b) Laboratoire des Matériaux, Surfaces et Procédés pour la Catalyse, LMSPC-ECPM, UMR CNRS 7515, Université de Strasbourg, 25 rue Becquerel, 67807 Strasbourg, France

## Abstract

The effect of the magnesia loading on the surface structure and catalytic properties of NiSn/MgO–Al2O3 catalysts for hydrogen production by methanol steam reforming has been investigated. The catalysts have been obtained by impregnation of γ-Al2O3 by the incipient wetness method, with variation of the MgO content. X-ray diffraction (XRD), BET surface area and H2-temperature programmed reduction (TPR) have been used to characterise the prepared catalysts. From this, it has been concluded that the incorporation of MgO results in the formation of MgAl2O4 spinel, which modifies the acid–base properties of the catalysts. The formation of Ni–Sn alloys after the reductive pre-treatment has also been evidenced.

The influence of the temperature of reaction and of the MgO loading on the hydrogen production by reforming of methanol has been established. Moreover, tests of catalytic stability have been carried out for more than 20 h. The carbonaceous deposits have been examined by temperature-programmed oxidation (TPO). The analysis of the catalysts after reaction has confirmed the low level of carbon formation on these catalysts. In no case, carbon nanotubes have been detected on the solids.

## Keywords

H2 production; Methanol; Steam reforming; Nickel catalysts; Magnesia; Alumina

## 1. Introduction

Currently, much attention is focused on fuel cells as a clean and efficient source of electrical power for both mobile and stationary applications [1] and [2]. Fuel cells generate electrical power by electrochemical oxidation of hydrogen with atmospheric oxygen. Hydrogen, which is a clean, storable and renewable fuel that does not produce pollutants or greenhouse gases upon combustion, is potentially a major fuel for internal combustion engines and fuel cells in the future.

Several processes, such as steam reforming, autothermal reforming, partial oxidation and water gas shift, can be used to extract hydrogen from fuels like gasoline, diesel, methane, methanol and ethanol. Because of its high hydrogen to carbon ratio (4) and because it can be obtained either from fossil resources or from biomass, methanol is one of the most promising sources for hydrogen production [3] and [4], mainly by steam reforming.

$$CH_3OH + H_2O \rightarrow 3H_2 + CO_2; \quad \Delta H^{\circ}_{298} = 47.7\ \text{kJ mol}^{-1}$$

As a liquid fuel to produce hydrogen, methanol shows some advantages in comparison with other hydrocarbons, such as its relatively low reforming temperature (250–350 °C), its lower sulphur content (<5 ppm) and its ease of handling [5]. All these properties make the methanol an interesting fuel to be used in steam reforming process applied to the emerging microchannel technology mainly focused to applications in portable power sources [6], [7], [8] and [9]. However, microchannel reactors can have some disadvantages when their use in commercial practice is considered. The catalysts cannot be easily replaced upon deactivation and the small channels are submitted to the risk of blockage due to carbon formation [10]. Hence, adequate catalysts to be used in the microreformer showing high activity and, specially, a very good stability in order to avoid the carbonaceous deposits typically formed on the reforming catalysts that may result in plugging of the reformer microchannels are needed.

Despite the deactivation due to coke formation on their surface, Ni-based catalysts have been widely used in conventional steam reforming processes [11], [12], [13], [14], [15], [16], [17] and [18]. Coking of Ni catalysts is fairly well understood: hydrocarbons dissociate on the metal surface producing adsorbed carbon that can be either gasified to produce carbon oxides or polymerise to give rise to carbon species that accumulate on the surface or dissolve in the metal, this dissolution process being essential for the formation of carbon whiskers [19]. In addition to these whiskers, surface deposits may result in ordered structures that encapsulate and hence deactivate the catalyst.

Among the strategies to avoid metal dusting and carbon growth, alloying Ni with metals less reactive towards carbon including noble metals [19], [20], [21], [22], [23] and [24], and selective poisoning of the active surface sites by sulphur have been proposed [25]. An industrial approach was developed using this later idea (SPARG process) [26].

Trimm [19] hypothesizes that the similar electronic structure of carbon and elements of groups IV and V of the periodic table may favour the interaction of these metals with Ni 3d electrons, thereby reducing the chance of nickel carbide formation. Although the formation of nickel carbide has been discarded as the initial step in the metal dusting process of nickel alloys [21], recent first-principle calculations on the adsorption of CO, OH, C and H on Ni3Sn surfaces has pointed out that the adsorption energy of these species depends on the presence of tin as nearest or next-nearest neighbour of the nickel atoms [27]. These results are in agreement with recent work by Nikolla et al. [28] and [29] that shows that the barrier for C–C bond formation increases with doping with tin Ni (1 1 1) and (2 1 1) surfaces. Their DFT studies let them establish that for the 1:3 Ni:Sn ratio the most stable surface stoichiometry is achieved.

Shabaker et al. [30] proposed a model particle for Ni–Sn/Al2O3 catalysts consisting of a Ni3Sn phase around a core of Ni. Evidence for the formation of the alloy was obtained by Mössbauer spectroscopy [31] and [32]. These authors conclude that their catalysts consist of a Sn-rich surface surrounding a core of Ni that adsorbs CO and H2 more weakly than Ni alone, in good agreement with surface science studies of NiSn alloys [33]. However, according to Saadi et al. [27], no experimental proof of the stoichiometric composition Ni3Sn during a metal dusting investigation is reported in the literature so far.

Alternatively, coking may be reduced by gasifying the deposited carbon species [34], [35] and [36]. The modification of the support by adding alkaline components such as MgO, K2O [37] or lanthanide oxides [38] and [39] favour the gasification of coke. The combination of adding a basic promoter and an alloying element of nickel catalysts must result in favouring coke-resistant Ni catalysts for the steam reforming of hydrocarbons.

In this paper, part of a wide study devoted to the design of catalysts for the steam reforming of biomass-derived fuels, a series of nickel catalysts supported on magnesia-modified γ-Al2O3 supports have been prepared allowing the study of the influence of the support acid–base properties on coke deposition. In every case, the active nickel phase was alloyed with tin keeping a 3:1 Ni:Sn weight ratio, the tin capacity to form alloys with nickel should result in minimization of the coking process. The steam reforming of methanol was chosen as a test for evaluating catalytic activity and carbon deposition.

## 2. Experimental

### 2.1. Supports and catalysts preparation

A series of NiSn/MgO–Al2O3 catalysts having a 15 wt.% NiSn loading with a 3:1 Ni:Sn weight ratio and variable MgO loadings (0, 5, 10 and 30 wt.%) were prepared by the incipient wetness method. Aqueous solution of magnesium nitrate hexahydrate (Mg(NO3)2·6H2O, Aldrich) was impregnated onto micrometric γ-Al2O3, followed by drying overnight at 120 °C in an oven. The resulting solid was further impregnated with

an aqueous solution of nickel (II) nitrate hexahydrate ($Ni(NO_3)_2 \cdot 6H_2O$, PANREAC) and anhydrous tin (II) chloride ($SnCl_2$, Fluka). After impregnation, the catalysts were dried at 120 °C overnight and finally calcined at 700 °C for 12 h in flowing 0.1% NOx/He/10% $H_2O$/synthetic air. Since the catalysts are synthesized from nitrate solutions, the calcination process is performed in NOx atmosphere in order to get better dispersion of Ni particles.

The supports will be named as 0MgAl, 5MgAl, 10MgAl and 30MgAl according to their MgO content (wt.%), and similarly, the catalysts will be referred as NiSn/0MgAl; NiSn/5MgAl; NiSn/10MgAl and NiSn/30MgAl.

### 2.2. Characterization techniques

X-ray diffraction (XRD) analysis was carried out in a Siemens D500 diffractometer. Diffraction patterns were recorded using Cu Kα radiation (40 mA, 40 kV) and a position-sensitive detector using a step size of 0.05° and a step time of 1 s.

The textural properties were studied by $N_2$ adsorption–desorption isotherms at liquid nitrogen temperature. The experiences were carried out in a Micromeritics ASAP 2010 equipment. Before analysis, the samples were degassed for 2 h at 150 °C in vacuum.

Temperature programmed reduction (TPR) was carried out in order to identify the reduction temperature and $H_2$ uptake of the catalysts. TPR experiments were performed using 0.05 g of the catalysts at the heating rate of 15 °C/min from room temperature to 900 °C, under a hydrogen/argon mixture (52 mL/min, 3.85%, v/v).

Temperature programmed oxidation (TPO) of the reacted catalysts, after methanol steam reforming, were carried in order to investigate the carbonaceous deposits on the catalysts. The TPO experiments were performed using 0.05 g catalyst in an oxygen/helium mixture (50 mL/min, 10% (v/v)), heated from room temperature to 800 °C at 15 °C/min. The $CO_2$ formed was followed by mass spectrometry and its quantification permitted to determine the total quantity of carbon on the analysed sample.

FT-IR spectra of adsorbed pyridine were recorded on a Nicolet Avatar 380 FT-IR spectrometer equipped with a DTGS detector. The samples were pressed into self supporting discs, placed in a quartz IR cell and treated under vacuum ($10^{-6}$ Torr) at 600 °C for 1 h. After cooling at room temperature, the samples were exposed to subsequent doses of pyridine after surface saturation. The, the spectra (128 scans, 2 $cm^{-1}$ resolution) were recorded.

### 2.3. Catalytic test

The methanol steam reforming catalytic test was carried out in a fixed bed reactor at atmospheric pressure. The catalyst was reduced in situ before reaction. The samples (0.16 g) were pretreated in 3 mL/min hydrogen flow (5%, v/v $H_2$:Ar) from RT to 800 °C (5 °C/min) and maintained under these conditions for 1 h. Then, the hydrogen flow

was suspended, and an Ar:N2 mixture (total flow of 2.3 L/h, 4:1 M) was admitted until total hydrogen purge and the temperature was decreased to the reaction one (350 °C). Finally, the reaction mixture methanol/water (1/2 molar ratio, 0.7 L/h of mixture in gas phase) was introduced in the reactor. In all the experiences the space velocity (GHSV) was 26,000 h−1. The effluent compounds were analysed on line by gas micro-chromatograph with two channels (Poraplot Q and molecular sieve 5 Å). Empty reactor and loaded with pure supports showed no activity under these conditions.

## 3. Results and discussion

### 3.1. Characterization of fresh catalysts

#### 3.1.1. Textural properties

The textural properties (SBET, and pore size and volume) of the supports and catalysts are summarized in Table 1.

The alumina support has the highest BET surface area and, after MgO addition the BET surface area and pore volume continuously decrease with the MgO loading. The BET surface area decreases linearly from 157 to 65 m2 g−1with the MgO loading for the 0MgAl, 5MgAl and 10MgAl, while a slight deviation from this linearity is detected for the support containing 30 wt.% of MgO (30MgAl). This suggests that the basic element is being incorporated into the pores of the alumina forming a less porous solid, as also reported in literature [40]. The pore volume and size values (Table 1) also confirm this idea. The pore size distribution of the supports is presented in Fig. 1. Pure alumina presents pores of about 38, 8 and 3 nm. The incorporation of MgO induces the almost disappearance of the pores at 38 nm and a loss of the proportion of the pores at 8 nm, demonstrating that MgO is deposited mainly in the pores of higher diameters.

The same argument may be invoked for the modification detected in the SBET after the NiSn incorporation, since the decrease in surface area is roughly the same in all the cases, except for the sample NiSn/30MgAl, in which a lower value is measured. Concerning the average pore size, it decreases deeply after NiSn addition on the Al2O3 support, but remains almost unchanged for all the supports with MgO.

#### 3.1.2. X-ray diffraction analysis

Both supports and catalysts were characterised by XRD in order to determine the modifications provoked by the MgO and active phase incorporation. Moreover, the catalysts were analysed after reductive process to determine the properties of the final solid used in the reforming reaction.

The XRD patterns of the prepared supports are shown in Fig. 2. The pure Al2O3 support shows all the characteristic diffraction lines corresponding to the (4 4 0), (4 0 0) and (3 1 1) planes of the gamma phase of the alumina at 66.79°, 45.76° and 37.58°, respectively; on adding MgO the diffraction lines shift continuously to lower 2θ values appearing at 65.57°, 45.00° and 36.89°, respectively, for the 30MgAl sample. This shift

must be ascribed to the formation of a spinel or a magnesium-defective spinel since it has been shown that the diffraction angle varies smoothly with the magnesium content [41]. The modification of the 2θ values observed upon magnesium addition is shown in Fig. 2. For the high MgO loaded sample, the 2θ values for the diffraction lines corresponding to the (4 4 0), (4 0 0) and (3 1 1) planes of the spinel structure fit quite well with those expected for the MgAl2O4 phase, Table 2. In addition to this, the presence of a MgO phase in the case of the 30MgAl sample is evidenced by the presence of diffraction lines at 42.97 and 62.29°. The Mg content for an "ideal" spinel phase (expressed as MgO percentage) is ca. 28 wt.%, therefore the 30MgAl sample contains an excess of magnesium in relation to the required amount to completely transform the alumina into the spinel phase. This excess of magnesium remains in the solid as magnesium oxide (42.97 and 62.29°) explaining the presence of diffraction peaks for this phase in the XRD pattern of the 30MgAl support.

As previously reported [41], the 2θ angles for the diffraction lines corresponding to the (4 4 0), (4 0 0) and (3 1 1) planes of the spinel structure shift to lower values as the MgO content of the supports increases, Fig. 2, reaching a plateau for MgO contents ranging 15–20 wt.% MgO. This pointing to the formation of support particles consisting in a γ-Al2O3 core surrounded by an outer MgAl2O4 phase layer for MgO loadings above 15 wt.%.

Although γ-Al2O3 may expose several crystal planes at the surface, it is assumed that the (1 1 0) and (1 0 0) planes are preferentially exposed, resulting in a saturation coverage after evacuation at 500 °C of 7.2 OH nm−2 as reported from molecular-dynamics simulation and experimental data [42] and [43]. If we assume that every OH surface group may hold Mg cations upon MgO addition, a MgO monolayer on top of the alumina surface will be formed after ca. 8% MgO loading. Thus, the observed plateau in Fig. 2 starting at 15–20 wt.% of MgO should be the consequence of the formation of a MgAl2O4 spinel layer on top of the alumina particle thick enough for preventing further incorporation of magnesium into the γ-Al2O3 bulk.

These results evidence that contents of magnesium oxide lower than 15–20 wt.% are well incorporated into the support structure and therefore, a modification of the acid–base properties of the bare support is ensured, which agrees with the literature data [20]. This fact is extremely important from a stability point of view in hydrocarbons reforming reactions, since a decreasing of the number of acidic sites decreases the coke formation on the solid [40].

The XRD patterns of the NiSn catalysts are shown in Fig. 4. The NiSn catalyst prepared using the alumina bare support present diffraction lines at 66.32, 45.47 and 37.36° which are shifted to lower angles with respect to the diffraction lines of the alumina support. In this XRD pattern, diffraction lines corresponding to NiO species (43.30 and 62.90°, see Table 2) are not observed.

These observations indicate that a nickel aluminate with spinel structure is formed (Table 2). In this case, the added amount of nickel (≈11 wt.%) is not enough to transform all the γ-Al2O3 into NiAl2O4 in which, the Ni content is around 33 wt.%. Therefore, a surface NiAl2O4 spinel should co-exists with the γ-Al2O3 support.

The NiSn catalyst supported on the 5MgAl support shows diffraction lines corresponding to the (4 4 0), (4 0 0) and (3 1 1) planes slightly shifted towards smaller angles than the corresponding support, Table 2. This indicates that nickel cations are incorporated into the γ-Al2O3 support resulting in a NixMgyAl2O4 surface phase. The support may accommodate up to 15–20 wt.% of divalent cations, Fig. 3, and therefore the 5 wt.% of MgO in addition to the 11 wt.% of NiO would be enough for forming a continuous MgNi–spinel layer on the surface of the γ-Al2O3. In addition to this, incipient diffraction lines corresponding to a NiO phase are clearly seen, Fig. 4. The catalyst prepared on the 10MgAl support presents diffraction lines corresponding to the (4 4 0), (4 0 0) and (3 1 1) planes at the same angles than those observed for the 10MgAl support indicating that in this case, Ni cations are not incorporated into the surface MgAl2O4 support. The presence of diffraction lines at 43.33 and 62.77° indicates the presence of a NiO phase supported on the MgAl2O4.

A similar behaviour is observed for the catalyst supported on the 30MgAl material showing the presence of diffraction lines at 65.66, 45.09 and 37.17° unmodified with respect to the pure support, together with two diffraction lines at 43.21 and 62.64° that are assigned to a (Mg,Ni)O solid solution. These two lines are shifted to higher angles with respect to the pure support and also shift to lower angles with respect to the NiSn/10MgAl catalyst, supporting the presence of the solid solution on top of a surface layer of MgAl2O4. A schematic representation of the materials particle structure is shown in Fig. 5.

The formation of this spinel phase is in agreement with a previous work by Jacob and Alcok [44] who studied NiAl2O4–MgAl2O4 solids solutions and proposed expressions (1) and (2) to calculate the free energy of formation of MgAl2O4 and NiAl2O4, respectively.

$$\Delta G^{\circ}\,(\text{cal mol}^{-1}) = -7000 - 0.7T \qquad (1)$$

$$\Delta G^{\circ}\,(\text{cal mol}^{-1}) = -1499 - 2.13T \qquad (2)$$

These equations evidence the preferential formation of MgAl2O4 at the temperature at which the catalysts have been calcined (700 °C), thus corroborating the previous hypothesis: For MgO contents lower than 28%, the coexistence of MgAl2O4 and NiAl2O4 spinels is possible, while if the MgO quantity is higher than this value, only the magnesium spinel is formed, remaining the excess of Mg and Ni in form of MgO–NiO solid solution, due to the high temperature of calcination and the complete miscibility of MgO and NiO phases [45], [46] and [47].

Diffraction peaks associated to Sn and/or NiSn phases were not detected in any case, probably due to the low concentration of tin in the samples (3.75% wt.%) and/or to its high dispersion or amorphous character.

XRD results suggest that the preparation method is adequate to incorporate a basic element (Mg) into the alumina support, modifying the surface structure resulting in a modification of the acid–base properties of the support, as desired. This fact has been evidenced by a detailed FTIR study carried out by Aupretre et al. [40] on similar catalytic supports. However, it is needed to consider that the catalysts are treated in a H2 flow before reaction, which may induce further transformations of the solids.

In order to demonstrate the decrease of the acid properties of the support after MgO incorporation, a FT-IR study of pyridine adsorption on the prepared solids has been performed (Fig. 6). All observed bands in all solids are characteristic of pyridine adsorbed on Lewis acid centers of the solid; no evidences of Bronsted centers capable of adsorbing pyridine to form PyH+ species (characterized by IR bands at about 1540 cm−1) are detected.

From the figure, it is clear that the introduction of MgO induces a decrease in the area of all bands, pointing out the decrease in the number of the Lewis acid sites of the support. In special, it is evident the loss of the band at 1622 cm−1 characteristic of pyridine adsorbed on Ia-type Al3+ tetracoodinated centers [48]. The disappearance of this band must be related with a decrease in the Lewis acidity of the solids after MgO incorporation.

In the case of the NiSn catalysts (not shown), similar results and trends are obtained, but the acidity of the samples are lower than those of the corresponding supports, because the metallic cations are placed in the free positions of the spinel structure.

### 3.1.3. H2-TPR analysis

Temperature programmed reduction (TPR) profiles obtained for NiSn/MgO–Al2O3 catalysts are presented in Fig. 7.

The NiSn/0MgAl catalyst shows three reduction peaks at 437, 570 and 798 °C. According to literature, the two first peaks are due to the presence of particles of NiO with different sizes [49]. The low peaks at 437 °C may be due to the reduction of NiO with the smaller crystallite size. The reduction peaks at higher temperatures are related to the reduction of NiO species with strong interaction with the support. The feature at 798 °C is undoubtedly due to the NiAl2O4 spinel reduction [44]. For the support containing a 5% of MgO, the TPR profile shows peaks at higher temperatures (510, 740 and 830 °C), meaning that the interaction of the reducible species (nickel) with the support is more important in this case. From a 10% of magnesium in the support, the peak at 740 °C shift to 718 °C and increases its intensity, suggesting that in this case, the quantity of reducible nickel species is higher that previously and its interaction with the support is weaker. This fact reflects that the MgAl2O4 is the major component and a part of nickel is now as NiO species strongly interacting with the support. It is needed to consider in this point that XRD peaks attributed to NiO (or MgO) were detected for this

composition. Taking into account that MgO is a non-reducible species, one can attribute these peaks to NiO species strongly interacting with the support. Finally, the TPR profile of the NiSn/30MgAl catalyst shows an important increasing (in area and temperature) of the peak at 778 °C. This fact confirms that the added magnesium is forming the MgAl2O4 spinel and the nickel is present as NiOx. Therefore, the magnesium addition to the γ-Al2O3 results in the MgAl2O4 spinel formation, which favours the interaction of reducible nickel with the support. The percentage of reduced nickel although increase when increasing the amount of MgO in the support, remaining always in the range 85–95%.

This aspect is easily understood considering that in an ideal MgAl2O4 spinel, the Mg/Al atomic ratio is 0.5 and in our case, the addition of 30% of MgO to the Al2O3 gives an atomic ratio of 0.4. For lower magnesium contents, part of the nickel content is forming the NiAl2O4 and therefore the quantity of nickel in the form of NiOx is low, as observed by the TPR peaks area. This fact again indicates that the formation of MgAl2O4 has to be more favourable from an energetic point of view [44] and support the structure for the catalyst particle schematised in Fig. 5.

In summary, all the calcined catalysts exhibit two principal groups of reduction peaks, at around 550 °C and at 800 °C, attributed to the reduction of nickel phases with different morphology and degree of interaction with the support. According to the literature, the reduction peaks at around 550 °C are due to the reduction of nickel present as NiO phase [49]. At temperatures higher than 800 °C, the peaks are assigned to the reduction of nickel incorporated into the major NiAl2O4 phase, while the peaks around 700 °C reflect the reduction of NiO species on the surface of nickel–aluminate spinels [44].

### 3.1.4. Characterization of reduced catalysts (after TPR)

In order to determine the changes in the crystalline phases produced by reduction, X-ray diffraction analyses were performed (Fig. 8).

From this figure, it can be observed that diffraction lines corresponding to alumina and spinel phases are still present. Moreover, peaks at 51° and 62° evidence the formation of metallic nickel during the reduction process. As in the case of the bare support, the shift of the peak positions to lower angles for growing magnesium contents indicates the presence of the spinel phase. It is noteworthy to stress the modifications of the peaks in the 40–50° region, where the peaks corresponding to different Ni–Sn alloy are reported [50]. It is clear that the diffraction lines in this region are being modified by the magnesium incorporation, where the appearance of a “new” peak at 45° (Fig. 8) is evidenced. This diffraction line (with low intensity for the free magnesium support) match with the most intense one of a Ni3Sn alloy (JPCDS 00-035-1362) and demonstrates the formation of such alloy, but the presence of NiSn and Ni3Sn4 alloys cannot be discarded. The higher intensity of these lines for higher magnesium contents also point to the preferential formation of MgAl2O4 spinel. Since the formation of this phase causes the increasing of the nickel species out of the structure (when the added

nickel quantity increases), its combination with the tin is provided, generating the detected metallic alloy. This fact was also evidenced by the TPR profiles: the reduction peaks of nickel species increases in intensity for the highest MgO loading.

Considering the ideas exposed in the introduction, the alloy formation between the nickel and an element with an electronic configuration similar to carbon (tin), is one of the main objectives of this work since it improves the resistance to the coking of the bimetallic catalyst. The stability of the catalysts was tested in the methanol steam reforming reaction.

### 3.2. Methanol steam reforming

Fig. 9 shows the H2 production as a function of the temperature (250–450 °C) in the steam reforming reaction for all the prepared catalysts, after reductive pretreatment. The value corresponding to the thermodynamic equilibrium is included to a comparative propose.

The performance of nickel-tin catalysts was found to be quite similar but an improvement in the hydrogen production was observed at higher temperatures for high MgO loadings. The lower performance detected for the NiSn/0MgAl and NiSn/5MgAl may be attributed to the presence of NiAl2O4 phase in these solids, which provokes a decreasing of Ni0 sites (active sites) generated after the reductive pre-treatment. The NiSn/30MgAl catalyst shows the highest hydrogen production at 450 °C (close to the thermodynamic value). The reason is also connected with the major fraction of reduced nickel (Ni0) in this sample, strongly depending on the quantity of added MgO because of the preferential formation of MgAl2O4 spinel phase compared with the NiAl2O4, as previously established from the XRD and TPR studies.

Considering that the tin addition to the catalysts was carried out in order to increase the coking resistance, a stability study of the solids was performed for more of 20 h. The chosen temperature was 350 °C because in these conditions, the hydrogen production is far enough from the thermodynamic value, to make sure that the activity measured is not limited by the thermodynamic and any modification in the hydrogen production is easily detected. As example, the evolution with time on stream obtained for the catalysts containing 5 wt.% and 30 wt.% MgO, respectively is presented in Fig. 10.

The only products detected for the NiSn/30MgAl catalyst were H2, CO and CO2. Besides them, dimethyl ether (DME) was observed for the NiSn/5MgAl (Fig. 10A) and NiSn/0MgAl (results not shown). This fact is not surprising because the DME is a product of the methanol dehydration, which is catalysed by the surface acid sites. Some authors [51] and [52] have recently evidenced the direct relation between the number of acidic sites on a catalyst (measured by NH3-TPD) and the DME production. In our case, the MgO addition provokes a decreasing of the number of acidic sites and so, the DME formation decreases with the MgO content, being not more detected from a MgO loading higher than 5 wt.%.

According to Fig. 10, the H2 production is slightly higher for the catalyst containing 30% MgO while the CO and CO2 productions are very similar in both cases. The reaction of methanol dehydration to produce DME provokes a decreasing of the reforming reaction extent, giving a lower hydrogen production. Therefore, one can affirm that the magnesium addition inhibits the by-products formation, mainly by decreasing the number of acidic sites, as demonstrated by FT-IR pyridine adsorption, so improving the selectivity of the steam reforming reaction.

### 3.3. Characterization of the catalysts after reaction

#### 3.3.1. X-ray diffraction analysis

The XRD patterns of the used catalysts showed a modification in the 40–50° region, indicating the modification of the type of Ni–Sn alloy during the reaction (figure not shown). Moreover, the presence of NiO and metallic tin is not discarded. Even if the nickel oxidation and Ni–Sn alloy modifications proceed in some extent, the results of activity (constant for about 20 h) indicate that these processes are not strongly affecting the catalytic process. XRF studies of the reacted samples show that no loss of tin is produced. Therefore, the analysis post-reaction will be mainly focused to study the poisoning of the catalyst by carbonaceous deposits.

#### 3.3.2. Study of carbonaceous deposits

The analysis of the carbonaceous deposits was carried out by temperature-programmed oxidation (TPO) of the catalysts (NiSn/5MgAl and NiSn/30MgAl) after 20 h of reaction. As it is know, this technique provides information about the quantity and nature of the coke formed on the solid. The amount of formed carbon was evaluated from the amount of CO2 (m/z = 44) produced during the TPO experiments (Fig. 11). The temperatures at which the maximum of CO2 production is observed informs about the type of carbonaceous species present on the catalysts.

TPO profiles of both catalysts show peaks of CO2 production at 350, and 465 °C. According to literature data [36], the peak at the lowest temperature is due to the combustion of CHx species or surface carbon, and the second one is produced by the oxidation of the nickel carbide. These authors consider that the combustion of carbon nanotubes gives a TPO peak at temperatures higher than 600 °C. In our case, peaks in this region are not observed, which indicates the absence of carbon nanotubes in the used solids. Taking into account that the reductive pre-treatment of the catalysts provokes the segregation of a Ni0 phase (Fig. 7), the nickel “carbide” formation (465 °C in TPO profiles) cannot be completely inhibited. However, it is appreciably decreased with the magnesium loading as shown in the TPO profile of the NiSn/30MgAl (Fig. 11). Moreover, it is observed that the quantity of CHx species or surface carbon (peak at 350 °C) is practically constant.

The measured quantities of carbon formed on the NiSn/5MgAl and NiSn/30MgAl were 25 and 22 μmol C/gcat respectively. On the one hand, the addition of magnesium to the alumina diminishes the carbon deposition, as a consequence of the basic properties of MgO [45] and [53]. This aspect has been widely studied by Aupretre et al. [40] studying ethanol steam reforming reactions. These authors explain that the coke formation is related with the alcohol dehydration on the acidic sites. Moreover, these authors clarify that this process is carried out on the support, while the dehydrogenation process (decreasing the quantity of coke) is carried out on both the support and the metal. In our case, the FT-IR study of pyridine adsorption confirms that the support modification with a basic element reduces the surface acidity and favours the low quantity of carbon formed.

On the other hand, the presence of Sn favours the stability of the catalysts due to the formation of an alloy with the nickel. However, the Sn quantity has to be optimised because a high activity is only reached at high temperature. Moreover, considering that the active phase load has been maintained constant in all the solids, the role of the MgO content may be inferred from the results. It has been observed that the catalyst containing the higher quantity of MgO forms a lower coke quantity (for a similar conversion), and that these carbonaceous species are not very stable, indicating the low degree of poisoning of the catalyst after 20 h under conditions of steam reforming reactions. This observation indicates that the MgAl2O4 spinel formation have to influence the coke gasification step, due probably to the high dispersion of the active phase and strong interaction with the support, facilitating the carbonaceous species oxidation.

## 4. Conclusions

Steam reforming of methanol was investigated over nickel supported catalysts on xMgO–Al2O3 (x = 0, 5, 10 and 30 wt.%). Characterization of the catalysts showed that the modification of alumina support by addition of MgO directly affects the surface composition of the catalysts, and the acid–base properties as a consequence. With increasing MgO loadings, a decreasing of the surface acidity of Al2O3 was deduced from the product distribution at the exit of the reformer and confirmed from FT-IR of adsorbed pyridine. Furthermore, the degree of nickel interaction with alumina was modified by formation of MgAl2O4 species, which inhibits the incorporation of nickel in the Al2O3 phase thus improving Ni dispersion. The sample containing 30 wt.% MgO exhibits the highest H2 yield and a high stability during 20 h of catalytic test. As a whole, the quantity of carbon formed is very low. The lower level of carbonaceous deposits on the Al2O3 with the highest MgO loading is related to the higher basicity of the support.

## Acknowledgments

A. Penkova and F. Romero-Sarria acknowledge the Spanish MEC for their contracts corresponding to the programs “Juan de la Cierva” and “Ramon y Cajal”. L. Bobadilla thanks the “Junta de Andalucía” for his research fellowship associate with the project

POG-TEP01965. The financial support by “Junta de Andalucía” (TEP106) and Spanish Ministerio de Ciencia e Innovación (ENE2009-14522-C05-01) co-financing by FEDER funds from European Union are gratefully acknowledged.

**References**

[1] W. Donitz

Int. J. Hydrogen Energy, 23 (1998), pp. 611–615

[2] D.R. Palo, R.A. Dagle, J.D. Holladay

Chem. Rev., 107 (2007), pp. 3992–4021

[3] C.N. Hamelinck, A.P.C. Faaij

J. Power Sources, 111 (2002), pp. 1–22

[4] G. Wu, T. Chen, W. Su, G. Zhou, X. Zong, L. Zhibin, L. Can

Int. J. Hydrogen Energy, 33 (2008), pp. 1243–1251

[5] Y.M. Lin, M.H. Rei

Catal. Today, 67 (2001), pp. 77–84

[6] L.M. Martinez, T.F. Romero-Sarria, M.I. Dominguez, M.A. Centeno, J.A. Odriozola, M. Montes

Aiche Spring National Meeting

American Institute of Chemical Engineers, New Orleans, LA, USA (2008) ISBN 978-0-8169-10, pp. 484–491

[7] Y. Men, G. Kolb, R. Zapf, D. Tiemann, M. Wichert, V. Hessel, H. Löwe

Int. J. Hydrogen Energy, 33 (2008), pp. 1374–1382

[8] J.D. Holladay, Y. Wang, E. Jones

Chem. Rev., 104 (2004), pp. 4767–4790

[9] G. Arzamendi, P.M. Dieguez, M. Montes, M.A. Centeno, J.A. Odriozola, L.M. Gandía

Catal. Today, 143 (2009), pp. 25–31

[10] A.K. Avci, D.L. Trimm, M. Karakaya

Catal. Today, 155 (2010), pp. 66–74

[11] J.K. Lee, D. Park

Korean J. Chem. Eng., 15 (1998), pp. 658–662

[12] D. Chen, R. Lodeng, K. Omdahl, A. Anundskgs, O. Olsvik, A. Holmen

Stud. Surf. Sci. Catal., 139 (2001), p. 93

[13] K. D: Ko, J.K. Lee, D. Park, S.H. Shin

Korean J. Chem. Eng., 12 (1995), pp. 478–480

[14] J.R. Rostrup-Nielsen

Catal. Today, 63 (2000), pp. 159–164

[15] O. Yokota, Y. Oku, T. Sano, N. Hasegawa, J. Matsunami, M. Tsuji, Y. Tamaura

Int. J. Hydrogen Energy, 25 (2000), pp. 81–86

[16] K.O. Christensen, D. Chen, R. Lødeng, A. Holmen

Appl. Catal. A, 314 (2006), pp. 9–22

[17] T. Borowiecki, A. Gołębiowski, B. Stasińska

Appl. Catal. A, 153 (1997), pp. 141–156

[18] C.H. Bartholomew

Appl Catal. A, 212 (2001), pp. 17–60

[19] D.L. Trimm

Catal. Today, 49 (1999), pp. 3–10

[20] Y. Nishiyama, K. Moriguchi, N. Otsuka, T. Kudo

Mater. Corros., 56 (2005), pp. 806–813

[21] J. Zhang, D.M.I. Cole, D.J. Young

Mater. Corros., 56 (2005), pp. 756–764

[22] A.M. Molenbroek, J.K. Nørskov, B.S. Clausen

J. Phys. Chem. B, 105 (2001), pp. 5450–5458

[23] F. Besenbacher, I. Chorkendorff, B.S. Clausen, B. Hammer, A.M. Molenbroek, J.K. Nørskov, I. Stensgaard

Science, 279 (1998), pp. 1913–1915

[24] A.K. Avci, D.L. Trimm, A. E: Aksoylu, Z.I. Önsan

Appl. Catal. A, 258 (2004), pp. 235–240

[25] H.J. Grabke

Mater. Corros., 54 (2003), pp. 736–746

[26] J.R. Rostrup-Nielsen

Sci. Technol., 5 (1984), pp. 1–117

[27] S. Saadi, B. Hinnemann, S. Helveg, C.C. Appel, F. Abild-Pedersen, J.K. Nørskov

Surf. Sci., 603 (2009), pp. 762–770

[28] E. Nikolla, A. Holewinski, J. Schwank, S. Linic

J. Am. Chem. Soc., 128 (2006), pp. 11354–11355

[29] E. Nikolla, A. Holewinski, S. Linic

J. Catal., 250 (2007), pp. 85–93

[30] J.W. Shabaker, D.A. Simonetti, R.D. Cortright, J.A. Dumesic

J. Catal., 231 (2005), pp. 67–76

[31] G.W. Huber, J.W. Shabaker, J.A. Dumesic

Science, 300 (2003), pp. 2075–2077

[32] J.W. Shabaker, G.W. Huber, J.A. Dumesic

J. Catal., 222 (2004), pp. 180–191

[33] C. Xu, B.E. Koel

Surf. Sci., 327 (1995), pp. 38–46

[34] Z.L. Zhang, X.E. Verykios

Catal. Today, 21 (1994), pp. 589–595

[35] O. Yamazaki, T. Nozaki, K. Omata, K. Fujimoto

Chem. Lett., 10 (1992), pp. 1953–1954

[36] K. Tomishige, Y. Chen, K. Fujimoto

J. Catal., 181 (1999), pp. 91–103

[37] D.L. Trimm, Z.I. Önsan

Catal. Rev., 43 (2001), pp. 31–84

[38] V. Meeyoo, J.H. Lee, D.L. Trimm, N.W. Cant

Catal. Today, 44 (1998), pp. 67–72

[39] V.A. Tsipouriari, Z. Zhang, X.E. Verykios

J. Catal., 179 (1998), pp. 283–291

[40] F. Aupretre, C. Descorme, D. Duprez, D. Casanave, D. Uzio

J. Catal., 233 (2005), pp. 464–477

[41] R. Basso, S. Carbonin, A. Della Giusta

Z. Kristallogr., 194 (1991), pp. 111–119

[42] L.J. Alvarez, J. Fernandez Sanz, M.J. Capitan, M.A. Centeno, J.A. Odriozola

J. Chem. Soc. Faraday Trans., 89 (1993), pp. 3623–3628

[43] H. Knozinger, P. Ratnasamy

Catal. Rev. Sci. Eng., 17 (1978), pp. 31–70

[44] K.T. Jacob, C.B. Alcok

J. Solid State Chem., 20 (1977), pp. 79–88

[45] A. Djaidja, S. Libs, A. Kiennemann, A. Barama

Catal. Today, 113 (2006), pp. 194–200

[46] J. Guo, H. Lou, H. Zhao, D. Chai, X. Zheng

Appl. Catal. A, 273 (2004), pp. 75–82

[47] P. Malet, M. Martin, M. Montes, J.A. Odriozola

Solid State Ionics, 95 (1997), pp. 137–142

[48] G. Busca, V. Lorenzelli

Mater. Chem., 7 (1982), p. 89

[49] J.T. Richardson, M.V. Twigg

Appl. Catal. A, 167 (1998), pp. 57–64

[50] H. Guo, S. Zhao, H. Zhao, Y. Chen

Electrochim. Acta, 54 (2009), pp. 4040–4044

[51] S.-M. Kim, Y.-J. Lee, J.W. Bae, H.S. Potdar, K.W. Jun

Appl. Catal. A, 348 (2008), pp. 113–120

[52] L. Wang, Y. Qi, Y. Wei, D. Fang, S. Meng, Z. Liu

Catal. Lett., 106 (2006), pp. 61–66

[53] K.Y. Koo, H.S. Roh, Y.T. Seo, D.J. Seo, W.L. Yoon, S.B. Park

Appl. Catal. A, 340 (2008), pp. 183–190

**Figure captions**

**Figure 1.** Pore size distribution on the considered supports.

**Figure 2.** XRD patterns of supports dryed at 120 °C overnight. (●) MgAl2O4, (♦) MgO

**Figure 3.** Fitting of the 2θ angle corresponding to the (4 4 0), (4 0 0) and (3 1 1) diffraction planes as a function of the magnesium content for the magnesia modified supports.

**Figure 4.** XRD patterns of the catalysts as a function of the MgO loadings in the support. (●) MgAl2O4 or NiAl2O4, (♦) MgO, NiO or NiO–MgO.

**Figure 5.** Schematic representation of the particle structure for the synthesised catalysts.

**Figure 6.** FT-IR spectra of pyridine adsorption at room temperature on the considered supports.

**Figure 7.** H2-TPR patterns of NiSn/MgO–Al2O3 catalysts as a function of MgO loadings.

**Figure 8.** XRD patterns of NiSn/MgO–Al2O3 catalysts after TPR. (●) Al2O3; (♦) MgAl2O4; (★)Ni; (♣) Ni–Sn alloys.

**Figure 9.** Hydrogen production as a function of temperature in the methanol steam reforming over catalysts with different MgO loadings.

**Figure 10.** Product distribution during the steam reforming of methanol at 350 °C: (A) NiSn/5MgAl and (B) NiSn/30MgAl.

**Figure 11**. TPO profiles of NiSn/5MgAl and NiSn/30MgAl (dash line).

**Table 1**

Table 1. Textural properties of supports and catalysts.

| **Sample** | $S_{BET}$ **($m^2/g$)** | $V_{pore}$ **($cm^3/g$)** | $D_{pore}$ **(Å)** |
|---|---|---|---|
| 0MgAl | 157 | 0.36 | 111 |
| 5MgAl | 137 | 0.26 | 75 |
| 10MgAl | 118 | 0.23 | 78 |
| 30MgAl | 65 | 0.14 | 87 |
| NiSn/0MgAl | 138 | 0.22 | 64 |
| NiSn/5MgAl | 113 | 0.21 | 74 |
| NiSn/10MgAl | 94 | 0.21 | 80 |
| NiSn/30MgAl | 52 | 0.11 | 89 |

**Table 2**

Table 2. Main diffraction lines for the prepared supports and catalysts.

| MgO (%) | Compound | $Al_2O_3$ | | | MgO | | NiO | | JCPS |
|---|---|---|---|---|---|---|---|---|---|
| | | (4 4 0) | (4 0 0) | (3 1 1) | (2 0 0) | (2 2 0) | (2 0 0) | (2 2 0) | |
| 0 | 0MgAl | 66.79 | 45.76 | 37.58 | | | | | |
| 5 | 5MgAl | 66.51 | 45.66 | 37.36 | | | | | |
| 10 | 10MgAl | 65.94 | 45.19 | 37.17 | | | | | |
| 30 | 30MgAl | 65.57 | 45.00 | 36.89 | 42.97 | 62.29 | | | |
| | NiSn/0MgAl | 66.32 | 45.47 | 37.36 | | | | | |
| | NiSn/5MgAl | 66.13 | 45.38 | 37.26 | | | 43.35 | – | |
| | NiSn/10MgAl | 65.85 | 45.09 | 37.17 | | | 43.33 | 62.77 | |
| | NiSn/30MgAl | 65.66 | 45.09 | 37.17 | | | 43.21 | 62.64 | |
| Diffraction lines from database | | | | | | | | | |
| 0 | γ-$Al_2O_3$ | 66.60 | 45.67 | 37.54 | | | | | 00-050-0741 |
| 11.36 | $Mg_{0.39}Al_{2.41}O_4$ | 66.34 | 45.45 | 37.34 | | | | | 00-048-052[a] |
| 28.34 | $MgAl_2O_4$ | 65.24 | 44.83 | 36.85 | | | | | 00-021-1152 |
| | $NiAl_2O_4$ | 65.54 | 45.00 | 37.01 | | | | | 00-010-0339 |
| | NiO | | | | | | 43.28 | 62.88 | 00-047-1049 |
| | MgO | | | | 42.92 | 62.30 | | | 00-045-0946 |

a From [42].

**Figure 1**

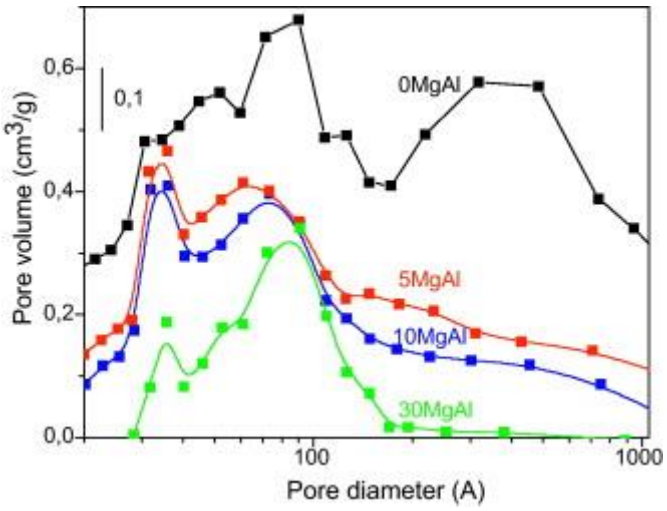
0,6
0,4
0,2
0,0
0,1
0MgAl
5MgAl
10MgAl
30MgAl
100
1000
Pore volume (cm3/g)
Pore diameter (A)

**Figure 2**

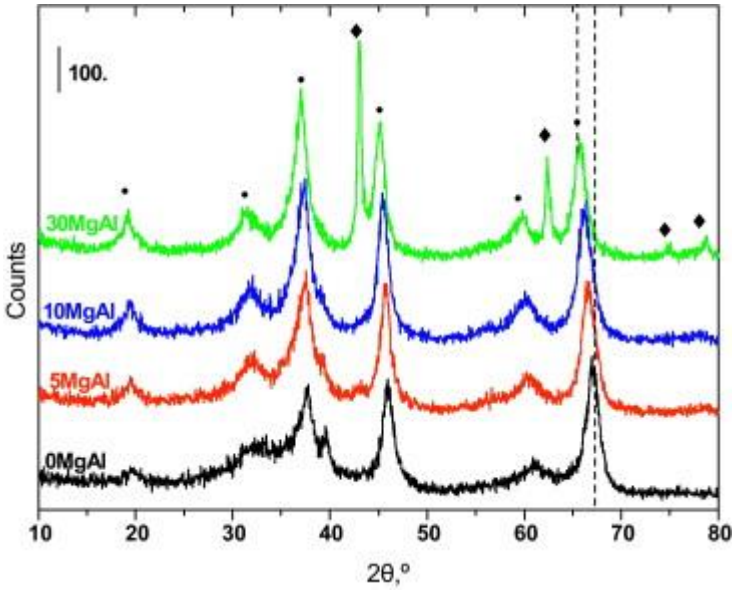

**Figure 3**

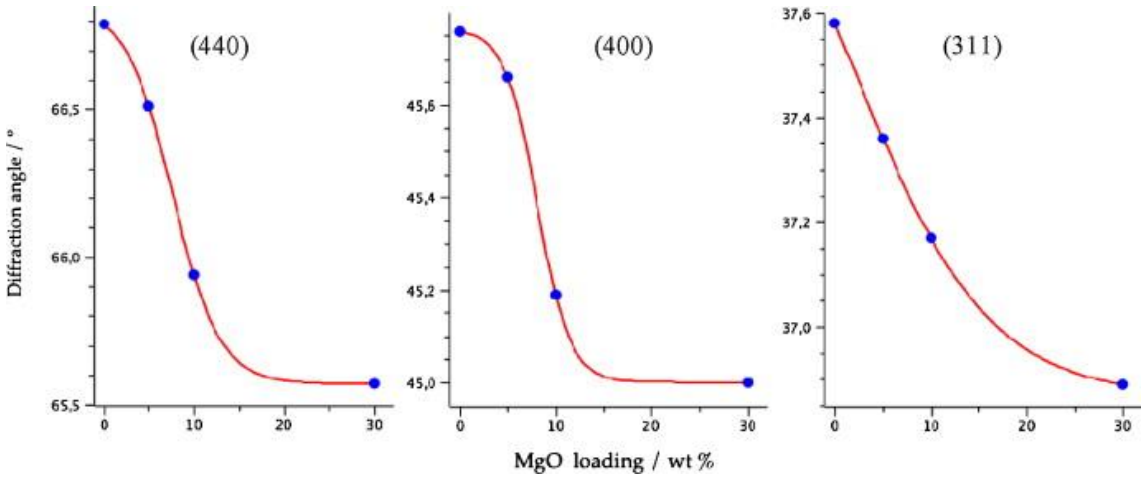
(440)
(400)
(311)
Diffraction angle / °
66,5
66,0
65,5
45,6
45,4
45,2
45,0
37,6
37,4
37,2
37,0
0
10
20
30
MgO loading / wt %

**Figure 4**

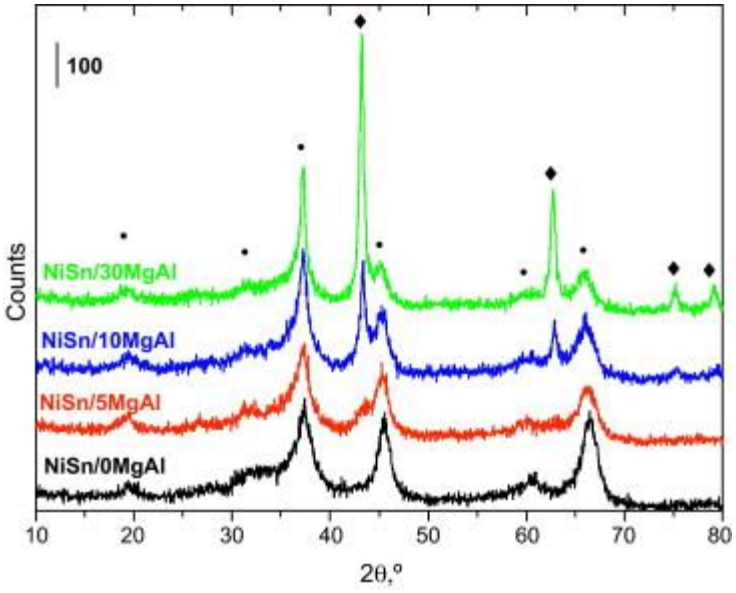
100
NiSn/30MgAl
NiSn/10MgAl
NiSn/5MgAl
NiSn/0MgAl
Counts
10
20
30
40
50
60
70
80
2θ,°

**Figure 5**

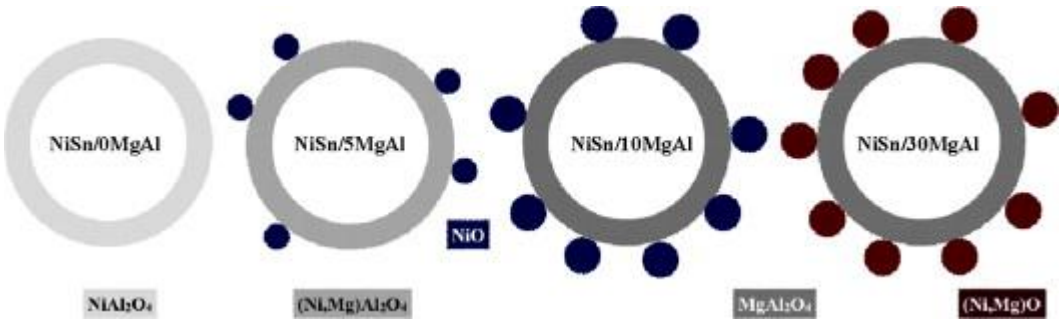
NiSn/0MgAl
NiSn/5MgAl
NiO
NiSn/10MgAl
NiSn/30MgAl
NiAl2O4
(Ni,Mg)Al2O4
MgAl2O4
(Ni,Mg)O

**Figure 6**

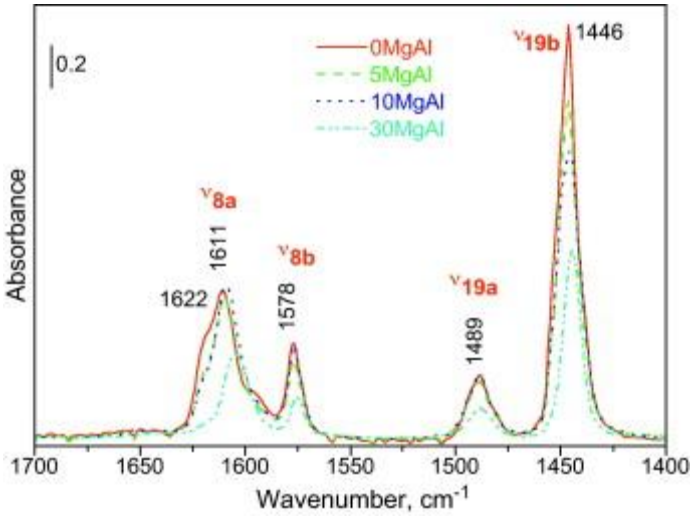
0.2
0MgAl
5MgAl
10MgAl
30MgAl
Absorbance
ν8a
1611
1622
ν8b
1578
ν19a
1489
ν19b
1446
1700
1650
1600
1550
1500
1450
1400
Wavenumber, cm-1

**Figure 7**

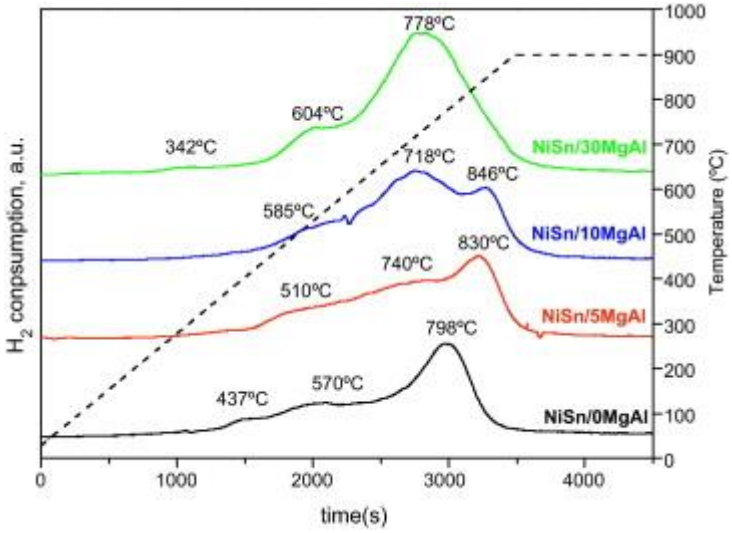
778°C
604°C
342°C
718°C
846°C
585°C
830°C
740°C
510°C
798°C
570°C
437°C
NiSn/30MgAl
NiSn/10MgAl
NiSn/5MgAl
NiSn/0MgAl
H2 conpsumption, a.u.
Temperature (°C)
time(s)
0
1000
2000
3000
4000
100
200
300
400
500
600
700
800
900
1000

**Figure 8**

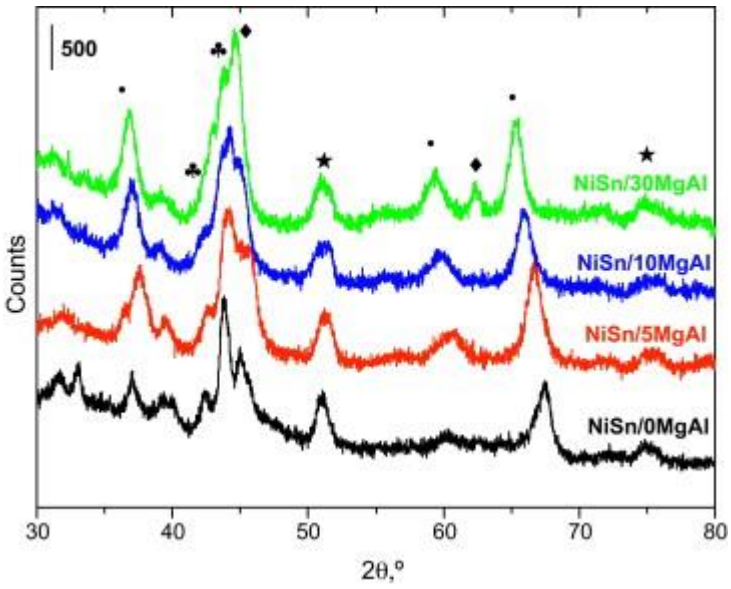
500
NiSn/30MgAl
NiSn/10MgAl
NiSn/5MgAl
NiSn/0MgAl
Counts
30
40
50
60
70
80
2θ,°

**Figure 9**

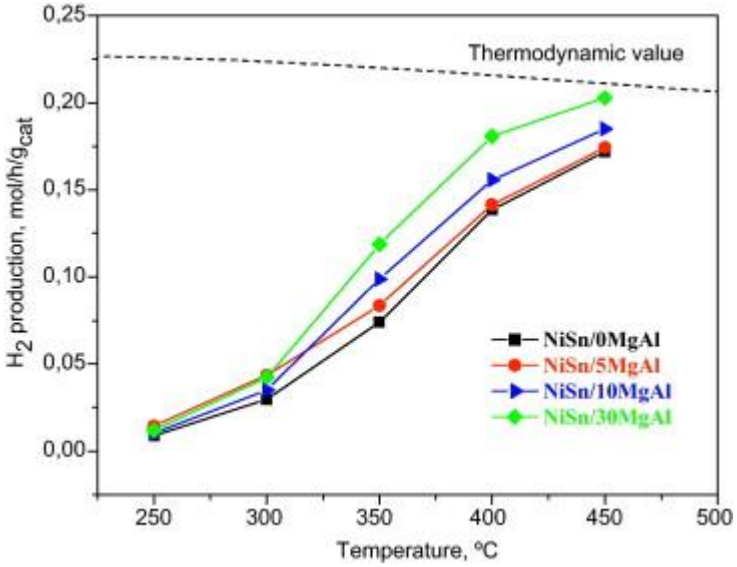
0,25
0,20
0,15
0,10
0,05
0,00
H2 production, mol/h/gcat
Thermodynamic value
NiSn/0MgAl
NiSn/5MgAl
NiSn/10MgAl
NiSn/30MgAl
250
300
350
400
450
500
Temperature, °C

**Figure 10**

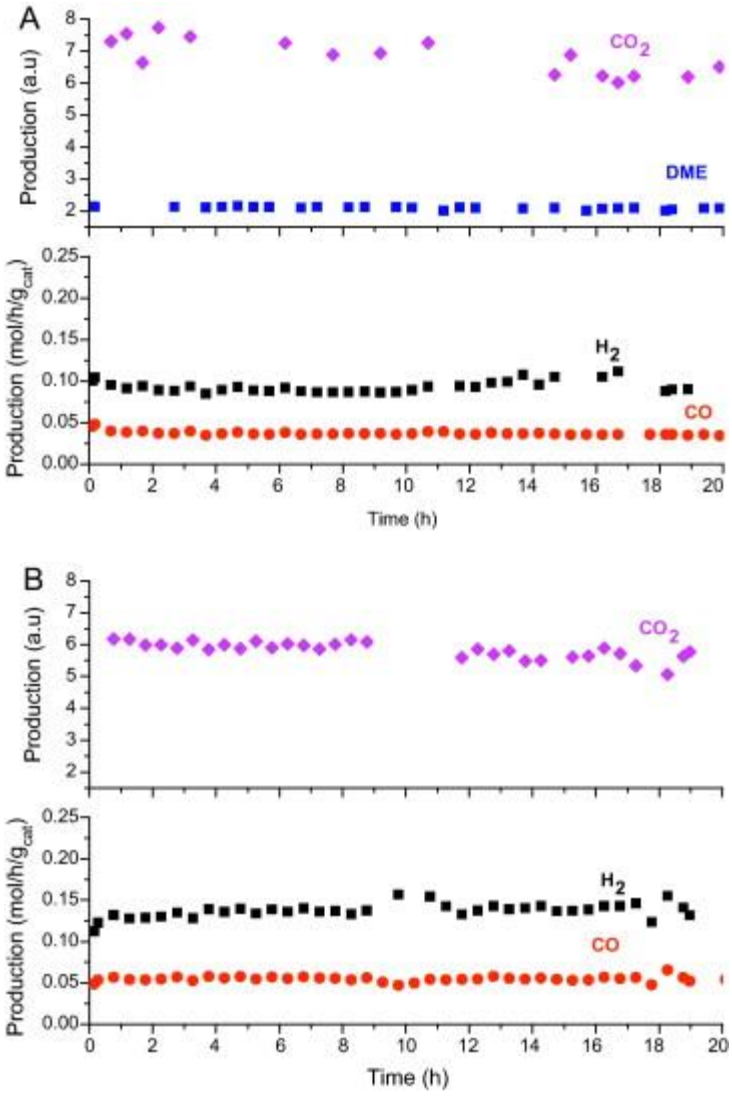
A
Production (a.u)
CO2
DME
Production (mol/h/gcat)
H2
CO
Time (h)
B
Production (a.u)
CO2
Production (mol/h/gcat)
H2
CO
Time (h)

**Figure 11**

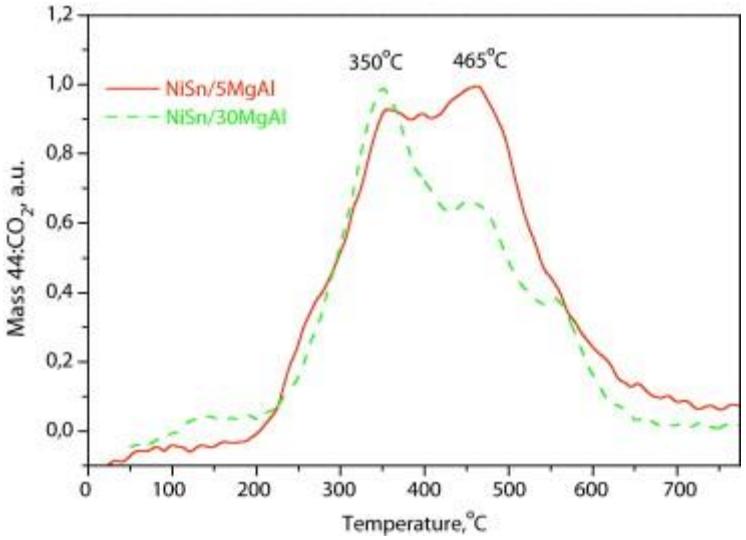
1,2
1,0
0,8
0,6
0,4
0,2
0,0
Mass 44:CO2, a.u.
NiSn/5MgAl
NiSn/30MgAl
350°C
465°C
0
100
200
300
400
500
600
700
Temperature,°C